This is the author's version of an article published in Electric Power Components and Systems. Changes were made to this version by the publisher prior to publication. DOI: http://dx.doi.org/10.1080/15325008.2015.1027017

Particle Swarm Optimization-based Superconducting Magnetic Energy Storage for Low Voltage Ride Through Capability Enhancement in Wind Energy Conversion System

[1]Hany M. Hasanien, and [2]S.M. Muyeen

[1]Electrical Power and Machines Department, Faculty of Engineering, Ain Shams University, 11517, Cairo, Egypt. (e-mail: hanyhasanien@ieee.org)

[2]Department of Electrical Engineering, The Petroleum Institute, Abu Dhabi, 2533, United Arab Emirates.

***Abstract*—This paper presents a novel application of the particle swarm optimization (PSO) technique to optimally design all the proportional-integral (PI) controllers required to control both the real and reactive powers of the superconducting magnetic energy storage (SMES) unit for enhancing the low voltage ride through (LVRT) capability of a grid-connected wind farm. The control strategy of the SMES system is based on a sinusoidal pulse width modulation (PWM) voltage source converter (VSC) and PI-controlled DC-DC converter. The control of VSC depends on the cascaded PI control scheme. All the PI controllers in the SMES system are optimally designed by the PSO technique. The statistical response surface methodology (RSM) is used to build the mathematical model of the voltage responses at the point of common coupling (PCC) in terms of PI controllers' parameters. The effectiveness of the PI-controlled SMES optimized by the proposed PSO technique is then compared to that optimized by genetic algorithms (GA) technique taking into consideration symmetrical and unsymmetrical fault conditions. Two-mass drive train model is used for the wind turbine generator system because of its large influence on the fault analyses. The paper demonstrates the systemic design approach in determining the controller parameters of SMES unit and validates its effectiveness in augmenting the LVRT of grid-connected wind farm.**

***Index Terms*— Genetic algorithms, low voltage ride through, particle swarm optimization, response surface methodology, squirrel cage induction generator, superconducting magnetic energy storage, wind energy conversion system.**

I. INTRODUCTION

THE wind power is considered nowadays one of the mainstream alternative sources of electricity generation. Many factors affect the huge growth of the wind power all over the world such as increase of fuel price, environmental concerns, and trend to a clean energy. The global wind power installations reached 238 GW at the end of 2011, bringing the total market growth of more than 20 % [1]. Based on the statistics of Global Wind Energy Council, it is expected that the wind power will contribute to 12 % of the total world electricity by 2020 [2]. These large grid-connected wind farms cause many power system problems which represent a challenging task for the researchers to solve it. One of the important problems adheres to grid-connected wind farms are a low voltage ride through (LVRT) capability enhancement.

The requirement of the LVRT applies to the wind power generators in order to remain stable and connected to the grid during the grid faults. Any disconnection of the wind power generators perhaps causes a critical grid situation and reduces the security standards especially when the wind penetration level is high. The recent wind farm grid codes insist on the LVRT characteristics of the wind power generators [3], [4]. As a result of US recent wind farm grid codes, the wind farm terminal voltage must return to 90 % of the rated voltage within 3 s after the start of the voltage drop, otherwise, the wind farm power station has to be shutdown [5].

Generally, squirrel cage induction generators are used as fixed-speed wind generators due to their merits such as simple operation, robust construction, cheapness, and low maintenance. Till now, fixed-speed wind farms represent around 40 % of total wind farm installations. Accordingly, the LVRT capability enhancement is still needed on such farms [6], considering a minimum of 20 years lifetime of wind turbines. This study focuses on the LVRT capability enhancement of a fixed-speed wind farm taking into consideration symmetrical and unsymmetrical network fault conditions by using particle swarm optimization (PSO) based superconducting magnetic energy storage (SMES).

Flexible AC transmission system (FACTS) devices such as a static synchronous compensator (STATCOM), static var compensator (SVC), and dynamic voltage restorer (DVR) have been used to solve

many power system problems. Recently, FACTS with an energy storage system (ESS) have been widely used for power system applications [7]. In [8], the LVRT capability of the wind farms was enhanced using STATCOM in comparison with thyristor controlled SVC. The STATCOM provides a better transient response than that of the SVC. However, the STATCOM is not capable of smoothing output power of the wind generator where it has not ability for active power control. Moreover, the LVRT capability of the wind generators was improved by using the DVR [9]. The DVR is considered a simpler solution than that of the STATCOM. However, using the DVR in the wind power generation has several problems such as a phase angle jump when a voltage dip in the network takes place. Therefore, specific control algorithms are used for this purpose [9]. The SMES unit has ability to enhance both of the LVRT and the power quality of the wind farms because of its flexibility in active and reactive power control.

Recently, the SMES system has received a great interest in the power system applications due to the huge development of superconductivity and power electronics. It has been used in the power quality enhancement, reactive power control, voltage control, and transient stability improvement [10]. It has many advantages such as fast response, high storage efficiency, and no restrictions on charging and discharging cycles [11]. However, it is still expensive and it is expected that its price will reduce in the near future.

Several studies have been performed to improve the transient stability of the wind generators using a proportional-integral (PI), fuzzy logic, and artificial neural network controllers [12] -[15]. However, the fuzzy logic controllers depend on the designer experience in tuning the membership functions and artificial neural network controllers suffer from the length of the training process. The PI controllers are the most widely used in industrial applications because of their robustness and offering a wide stability margin but they are sensitive to the nonlinear system dynamics. Therefore, fine tuning of the PI controllers is very difficult especially for large power system. Recently, in our previous studies, these controllers were fine tuned in wind energy conversion systems by Taguchi method which is a long statistical method and genetic algorithm (GA) method which is based on the concept of survival of the fittest [16]-[19].

In this study, the powerful swarm intelligence technique, PSO is used to optimally design all the PI controllers of the SMES unit used in a voltage source converter (VSC) and a DC-DC converter in controlling both the real and reactive powers to enhance the LVRT capability of a grid-connected wind farm. This represents the main contribution of this study and has so far not been reported in power system

literature. The LVRT analysis is carried out in the light of recent wind farm grid codes. The control strategy of the SMES system is based on a sinusoidal pulse width modulation (PWM) voltage source converter (VSC) and PI-controlled DC-DC converter. The control of VSC depends on the cascaded PI control scheme. All the PI controllers in the SMES system are optimally designed by the PSO technique. The statistical response surface methodology (RSM) is used to build the mathematical model of the voltage responses at the point of common coupling (PCC) in terms of PI controllers' parameters. The effectiveness of the proposed PI-controlled SMES optimized by the PSO technique is then compared to that optimized by GA technique taking into consideration symmetrical and unsymmetrical fault conditions. MATLAB optimization toolboxes are used for design optimization of the controllers' parameters. Two-mass drive train model is used for the wind turbine generator system because of its influence on the dynamic analyses. The validity of the proposed system is verified by the simulation results which are performed using the laboratory standard dynamic power system simulator PSCAD/EMTDC. Notably, the PI-controlled SMES optimized by PSO enhances the LVRT capability of a grid-connected wind farm.

II. MODEL SYSTEM

The system under study consists of a grid-connected fixed-speed wind farm, as shown in Fig. 1(a). The wind farm is modeled by the aggregated wind turbine model where many small size wind generators can be represented by a large capacity wind generator [20]. The wind farm is connected to the grid through a transmission line with double circuit. A capacitor C is connected to the wind farm terminals to compensate the reactive power at the steady state operation and its value has been selected to achieve unity power factor of the wind power station at the rated conditions. The parameters of the wind farm are illustrated in Table I [14]. The SMES unit is connected to the PCC.

III. Wind Turbine Model

The mechanical power extraction from the wind can be written as follows [21]-[24]:

$$P_w = 0.5\rho\pi R^2 V_w^3 C_P(\lambda, \beta) \quad (1)$$

where P_w is the mechanical power from the wind, ρ is the air density [kg/m^3], R is the blade radius [m], V_w is the wind speed [m/s], and C_p is the power coefficient which is a function of the tip speed ratio, λ, and blade pitch angle, β [deg.]. In this study, the C_p formula can be expressed as follows [25]:

$$\lambda = \frac{V_w}{\omega_B}$$

$$C_p = \frac{1}{2}(\lambda - 0.022\beta^2 - 5.6)e^{-0.17\lambda} \qquad (2)$$

where ω_B is the blade angular velocity [rad/s]. The turbine characteristics used are shown in Fig. 1(b). The two-mass drive train parameters of the wind generator are shown in Table I, where H_g and H_{wt} are the generator and wind turbine inertia constants, respectively, and K_w is the shaft stiffness between the two masses.

IV. SMES SYSTEM

In this study, the SMES unit consists of a three-phase Wye-Delta 66/0.77 kV transformer, a six pulse PWM VSC using insulated gate bipolar transistors (IGBTs), a DC-link capacitor of 60 mF, a two-quadrant DC-DC converter using IGBTs, and a superconducting coil of inductance 0.24 H, as shown in Fig. 2. The SMES unit is connected to the power system at the PCC. An over voltage protection system (OVPS) is used for the safety of the VSC unit and the capacitor. The braking chopper is modeled in the DC-link in order to protect the DC-link capacitor during the fault situation. The chopper is activated when the DC-link voltage increases over the predefined limit (20 % of the rated value) and dissipates the active power into the resistance during the voltage dip in the grid.

The stored energy, E [Joule], in the superconducting coil and its rated power, P [Watt], are described by the following equations:

$$E = \frac{1}{2} L_{sm} I_{sm}^2 \qquad (3)$$

$$P = \frac{dE}{dt} = L_{sm} I_{sm} \frac{dI_{sm}}{dt} = V_{sm} I_{sm} \qquad (4)$$

where L_{sm} is the inductance of the superconducting coil, I_{sm} is the DC current flowing through the coil, and V_{sm} is the instantaneous voltage across the coil. The rated values of E and P for the SMES system under

study are 0.05 MWH and 50 MW, respectively [14].

A. VSC

The VSC is a three-phase rectifier/inverter connecting the superconducting coil to the AC power system. The cascaded PI control scheme is used in this study, as shown in Fig. 3(a). The dq and three-phase electrical quantities are related to each other by the reference frame transformation. The transformation angle is detected from three-phase voltages (v_a,v_b,v_c) at the high voltage side of the transformer using a Phase-Locked Loop (PLL). The PI-1 controllers are used in the outer loops to follow the DC-link voltage (V_{DC}) error signal and the voltage at the PCC (V_{PCC}) error signal to produce $I_{d\text{-}ref}$ and $I_{q\text{-}ref}$, respectively. The PI-2 controllers are used in the inner loops to follow the I_d error signal and the I_q error signal to produce $V_{q\text{-}ref}$ and $V_{d\text{-}ref}$, respectively. These signals are converted to a three-phase sinusoidal reference waveform $V_{a,b,c\text{-}ref}$, which is compared with a triangular waveform to generate the gate signals of IGBTs. The frequency of the triangular waveform is selected 1 kHz. The V_{DC} is kept constant at 1 kV through the simulation using the PWM VSC.

B. DC-DC Converter

A two-quadrant DC-DC converter is used to control the DC voltage across the coil by adjusting its duty cycle. When the duty cycle is greater or lower than 50 %, the DC voltage is positive or negative and the coil is charged or discharged, respectively. Moreover, at 50 % duty cycle, the net DC voltage across the coil is zero and this means that the coil is neither charged nor discharged. The line power (P_L) is defined as the active power from the wind farm at the PCC. Fig. 3(b) shows the duty cycle control of the DC-DC converter. The PI-3 controller is used to follow the P_L error signal to update the duty cycle signal (D) which is compared with a triangular waveform to produce the gate signals for the IGBTs of the DC-DC converter. The chosen frequency of the triangular waveform is 1 kHz. In this study, all the PI controllers in the SMES system are optimally designed by the PSO technique. This represents a fully design optimization of PI controllers in such system.

V. OPTIMAL DESIGN

A. The RSM

Recently, the RSM has received a great attention for electrical machines and power system

applications. It is a powerful statistical method used to create a mathematical model by obtaining the relationship between the design variables and the response [26]. In this study, PSCAD/EMTDC [27] is used for numerical simulations to provide the response. The maximum percentage undershoot (MPUS), the maximum percentage overshoot (MPOS), and the settling time (Ts) of the V_{PCC} profile are the responses. These are varied by the design variables variant. In the RSM, the second order model is used to obtain an accurate response. The response surface creation depends on the Box-Behnken design which has a lower number of design experiments than that of the central composite design and leading to the same modeling accuracy.

B. PSO Approach

The PSO is a swarm intelligence computation technique presented by Eberhart and Kennedy in 1995 [28]. It is inspired by the social behavior of bird flocking and fish schooling. It has several advantages over other optimization techniques such as less parameters to be adjusted, fast computational time, and derivative free algorithm. The PSO technique has been used to solve many power system optimization problems [29]-[32].

Let the design variables of an optimization problem are N. The swarm of P particles is initialized in which each particle is assigned a random position in the N-dimensional hyperspace, such that each particle's position corresponds to a candidate solution. In the PSO technique, each particle has two vectors, the position vector ($X_i = [x_{i1}, x_{i2}, \ldots, x_{iN}]$) and the velocity vector ($V_i = [v_{i1}, v_{i2}, \ldots, v_{iN}]$). Each particle updates its position based on its own best exploration, best swarm overall experience, and its previous velocity vector according to the following equations [33]:

$$v_i^{k+1} = \omega v_i^k + c_1 r_1 (pbest_i^k - x_i^k) + c_2 r_2 (gbest^k - x_i^k) \quad (5)$$

$$x_i^{k+1} = x_i^k + v_i^{k+1} \quad (6)$$

where c_1 and c_2 are two positive acceleration constants; r_1 and r_2 are two random numbers in a range of [0, 1]; ω is the inertia weight; $pbest_i^k$ is the best position of particle i achieved based on its own experience; $pbest_i^k = [x_{i1}^{pbest}, x_{i2}^{pbest}, \ldots\ldots\ldots, x_{iN}^{pbest}]$; $gbest^k$ is the best particle position based on overall swarm's experience; $gbest^k = [x_1^{gbest}, x_2^{gbest}, \ldots\ldots, x_N^{gbest}]$; and k is the iteration index.

C. GA Approach

GA is a random search technique used for solving several optimization problems in engineering applications. This search depends on the principle of survival of the fittest. Moreover, it uses techniques inspired by evolutionary biology such as natural selection, mutation, and crossover.

VI. Systemic Design Approach of Proposed Optimization Technique

Fig. 4 shows the flowchart of the proposed PSO approach. The following steps summarize the whole design strategy:

Step 1- Selection of Variables and Levels:

The proportional gain and integral time constant of the PI controllers in the SMES system are the design variables. X_1, X_3, and X_5 are the proportional gain of PI-1, PI-2, and PI-3, respectively. X_2, X_4, and X_6 are the integral time constant of PI-1, PI-2, and PI-3, respectively. These design variables have three levels. The levels (-1), (0), and (1) represent the minimum, average, and maximum values of the design variable, respectively. The design variables and levels are shown in Table II.

Step 2- Design of Experiments:

In this study, the RSM model is based on the standard Box-Behnken design in building the responses. The experiments frequency is established by using Box-Behnken design. In this analysis, there are 54 experiments for six design variables problem, as shown in Table III. This statistical design is performed using Minitab program [34].

Step 3- PSCAD Program Calculation:

The PSCAD program calculation is carried out for each experiment and the values of MPUS, MPOS, and T_s of the V_{PCC} profile are determined and stored in Table III.

Step 4- Creation of RSM Model:

The MPUS (Y_1), MPOS (Y_2), and T_s (Y_3) of the V_{PCC} profile are fitted by second order polynomial functions as follows:

$$
\begin{aligned}
Y_1 = {} & 56 + 0.277x_1 - 0.54x_2 + 0.008x_3 - 0.57x_4 - 4.3x_5 + 4.5x_6 \\
& + 0.38x_1^2 - 0.22x_2^2 + 0.99x_3^2 + 0.65x_4^2 + 0.1x_5^2 - 4.44x_6^2 \\
& + 0.06x_1x_2 + 0.06x_1x_3 - 0.35x_1x_4 - 0.04x_1x_5 + 0.06x_1x_6 \\
& + 0.06x_2x_4 + 0.72x_2x_5 - 1.43x_2x_6 + 0.04x_3x_4 - 0.01x_3x_6 \\
& + 0.05x_4x_5 - 0.28x_4x_6 - 1.31x_5x_6
\end{aligned} \tag{7}
$$

$$
\begin{aligned}
Y_2 = {} & 12.85 - 1.66x_1 - 0.37x_2 + 0.42x_3 + 3.28x_4 - 0.38x_5 - 0.16x_6 \\
& + 0.28x_1^2 - 0.2x_2^2 + 0.06x_3^2 - 0.25x_4^2 + 0.6x_5^2 + 0.04x_6^2 \\
& - 0.03x_1x_2 + 0.05x_1x_3 + 0.02x_1x_4 + 0.8x_1x_5 - 0.47x_1x_6 \\
& - 0.04x_2x_3 + 0.05x_2x_4 + 0.11x_2x_5 - 0.23x_2x_6 - 0.03x_3x_4 - 0.01x_3x_5 \\
& - 0.02x_3x_6 - 1.15x_4x_5 + 0.93x_4x_6 - 0.19x_5x_6
\end{aligned} \tag{8}
$$

$$
\begin{aligned}
Y_3 = {} & 2.85 - 1.66x_1 - 0.64x_2 - 0.8x_3 + 2.43x_4 - 1.3x_5 + 1.58x_6 \\
& + 0.82x_1^2 + 0.35x_2^2 - 0.37x_3^2 + 0.82x_4^2 + 0.06x_5^2 + x_6^2 \\
& + 0.33x_1x_2 + 1.38x_1x_3 - 1.34x_1x_4 - 0.09x_1x_5 - 1.62x_1x_6 \\
& + 0.18x_2x_3 - 0.42x_2x_4 + 0.76x_2x_5 - 1.37x_2x_6 - 0.4x_3x_4 + 0.11x_3x_5 \\
& - 0.92x_3x_6 - 2.22x_4x_5 + 1.64x_4x_6 - 1.37x_5x_6
\end{aligned} \tag{9}
$$

Step 5- PSO Approach:

The PSO technique is applied directly to the RSM model. In this study, MATLAB optimization Toolbox is used [35]. The MPUS (Y_1) is the objective function and both of MPOS (Y_2) and T_s (Y_3) are nonlinear constraint functions. The constraints of the optimized problem are described as follows:

- Design variables range is $3 \leq X_1 \leq 5$, $0.08 \leq X_2 \leq 0.12$, $1 \leq X_3 \leq 2$, $0.001 \leq X_4 \leq 0.003$, $0.1 \leq X_5 \leq 1.1$, and $0.002 \leq X_6 \leq 0.5$.
- The MPOS constraint $Y_2 \leq 10\ \%$ and T_s constraint $Y_3 \leq 1.5\ s$.

The PSO characteristics are shown in Table IV. After 400 iterations, the PSO is terminated. Fig. 5 shows the fitness function convergence. Table V shows the optimization set value and level of the design variables. At these optimal values, the MPUS is 54.66 %, the MPOS is 8.9 %, and T_s is 1.02 s.

Step 6- GA Approach:

For a fair comparison, GA technique is also applied to the RSM model. In GA analysis, the Rank fitness scaling is applied to avoid premature convergence. GA includes natural selection, mutation, and crossover. The selection process is performed using the uniform selection technique which prevents bias

and minimal spread. The GA characteristics are illustrated in Table VI. GA optimization was terminated after the 5th iteration where the average change in the fitness value and the constraint violation were less than 1e-6. Fig. 6 shows the fitness function convergence and current best individual. The optimal level and size value of the design variables using GA technique are shown in Table V. Moreover, at these optimal values, the MPUS is 56.91 %, the MPOS is 9.5 %, and T_s is 1.5 s.

VII. Simulation Analysis and Discussion

In this study, the detailed switching model of a PWM VSC and DC-DC converter is considered for obtaining precise analyses. Two-mass drive train model is used for the wind turbine generator system because of its huge influence on the dynamic analyses. Time domain simulation has been done using PSCAD/EMTDC. The time step is 20 μs and the simulation time is 5 s. The wind speed is fixed at the rated value of 11.8m/s.

In this study, the simulation results are described in light of the recent grid code, set by E. On Netz, recently known as TenneT TSO GmbH [3]. Fig. 7 shows the LVRT standard of this grid code. The wind turbines are required to stay online and connected to the grid above the limit lines.

The system under study is subjected to a severe symmetrical three-line to ground fault (3LG) as a network disturbance. The fault occurs at 0.1 s at fault point F, shown in Fig. 1(a). The circuit breakers (CBs) on the faulted line are opened at 0.2 s to clear the fault, and are reclosed at 1 s.

Fig. 8(a) shows the voltage response at the PCC. It can be noted that without using the SMES unit, the voltage drop happens at the PCC causing sudden increase in the induction generator speed. As a result, the induction generator accelerates and becomes unstable. In contrast when SMES is used, the required reactive power is supplied from the VSC of the SMES unit properly according to the error signals and the voltage at the PCC can be returned back to the pre-fault level in a short time. Moreover, the DC-DC converter of the SMES unit controls the real power flow during the disturbance. It can be realized that the voltage response at the PCC when a PSO-based SMES unit is used, is a faster and better damped response than that obtained when a GA-based SMES unit is used. The induction generator and turbine speeds are illustrated in Figs. 8(b), and (c), respectively. Notably, the induction generator becomes stable with the

SMES unit. The line reactive and real powers at the PCC are shown in Figs. 8(d) and (e), respectively. The real power and stored energy of the SMES unit are shown in Figs. 8 (f) and (g), respectively. It can be noted that a better response and high storage efficiency are achieved with a PSO-based SMES unit than that of a GA-based SMES unit. Fig. 8 (h) shows the DC-link voltage response which has a better transient characteristic with a PSO-based SMES unit.

In fact, the better transient characteristics adhere to the PSO-based SMES unit is due to the merits of the PSO technique over GA technique. PSO has a perfect memory capability than GA. In addition, PSO is very effective in keeping the diversity of the swarm, since all the particles use the information related to the most successful particle to improve themselves, whereas in GA, the worse solutions are refused and only the good ones are accepted; therefore in GA the population has a part of the best individuals.

For further verification of the proposed control scheme, the transient analysis is performed using a most frequently occurred unsymmetrical fault (single-line to ground, 1LG) as a network disturbance. Fig. 8 (i) shows the voltage response at the PCC with this type of fault. It can be noted that the voltage response at the PCC with a PSO-based SMES unit is found better damped than that obtained with a GA-based SMES unit. It can also be claimed from the simulation results that PSO-based SMES unit works well for both symmetrical and unsymmetrical fault conditions. Not only the LVRT capability of a grid-connected wind farm can be improved but also the power quality can be enhanced using PSO-based SMES units.

VIII. CONCLUSION

This paper has presented the PSO technique for design optimization of all the PI controllers in a SMES unit to enhance the LVRT capability of a grid-connected wind farm. The LVRT is analyzed in light of the recent grid code set by E. On Netz, recently known as TenneT TSO GmbH. The SMES control strategy depends on a sinusoidal PWM cascaded-controlled VSC and PI-controlled DC-DC converter. The RSM has been used to build the mathematical model of the voltage responses at the PCC in terms of PI controllers' parameters in a precise way. The simulation results have shown that the system responses with a PSO-based SMES unit is faster and better damped than that of a GA-based SMES unit for both symmetrical and unsymmetrical fault conditions. The LVRT capability of a grid-connected wind farm can be noticeably improved using PSO-based SMES units. The proposed PSO based optimization methodology

for multiple PI controllers is also suitable for other power system applications including the FACTS, smart grid, and other renewable energy systems, especially when their transfer functions are difficult to be achieved.

REFERENCES

[1] Global Wind Energy Council (GWEC), "Annual market update 2011," Global Wind Report, online: http://www.gwec.net.
[2] Global Wind Energy Council (GWEC), "Global wind energy outlook 2012," online: http://www.gwec.net.
[3] E. On Netz, Grid Code, High and Extra-High Voltage, April 2006, available at www.eon-netz.com/.
[4] Bharat Singh and S. N. Singh, "Wind power interconnection into the power system: a review of grid code requirements," *The Electricity Journal*, vol. 22, no. 5, pp. 54-63, 2009.
[5] Federal Energy Regulatory Commission (FERC), United States of America, Docket No. RM05-4-000 – Order No. 661, "Interconnection for Wind Energy," Issued June 2, 2005.
[6] S. M. Muyeen, R. Takahashi, T. Murata, J. Tamura, M. H. Ali, Y. Matsumura, A. Kuwayama, and T. Matsumoto, "Low voltage ride through capability enhancement of wind turbine generator system during network disturbance," *IET Renewable Power Generation*, vol. 3, no. 1, pp. 65-74, 2009.
[7] Zhang L., Shen C., Crow M.L., Dong L., Pekarek S., and Atcitty S., "Performance indices for the dynamic performance of FACTS and FACTS with energy storage," *Electric Power Components and Systems*, vol. 33, no. 3, pp. 299-314, 2005.
[8] M. Molinas, Jon Are Suul, and T. Undeland, "Low voltage ride through of wind farms with cage generators: STATCOM versus SVC," *IEEE Transactions on Power Electronics*, vol. 23, no. 3, pp.1104–1117, May 2008.
[9] D. Ramirez, S. Martinez, C. A. Platero, F. Blazquez, and R. M. de Castro, "Low-voltage Ride-Through capability for wind generators based on dynamic voltage restorers," *IEEE Transactions on Energy Conversion*, vol. 26, no. 1, pp. 195–203, March 2011.
[10] Marcelo Gustavo Molina, and Pedro Enrique Mercado, "Power flow stabilization and control of microgrid with wind generation by superconducting magnetic energy storage," *IEEE Transactions on Power Electronics*, vol. 26, no. 3, pp. 910-922, March 2011.
[11] IEEE Task Force on Benchmark Models for Digital Simulation of FACTS and Custom-Power Controllers, T&D Committee, "Detailed modeling of superconducting magnetic energy storage (SMES) system," *IEEE Transactions on Power Delivery*, vol. 21, no. 2, pp. 699-710, April 2006.
[12] Mohd. Hasan Ali, Minwon Park, In-Keun Yu, Toshiaki Murata, and Junji Tamura, "Improvement of wind generator stability by fuzzy logic-controlled SMES," *IEEE Transactions on Industry Applications*, vol. 45, no. 3, pp. 1045-1051, May/June 2009.
[13] Li Wang, Shiang-Shong Chen, Wei-Jen Lee, and Zhe Chen, "Dynamic stability enhancement and power flow control of a hybrid wind and marine-current farm using SMES," *IEEE Transactions on Energy Conversion*, vol. 24, no. 3, pp. 626-639, September 2009.
[14] Hany M. Hasanien, Syed Q. Ali, and S.M. Muyeen, "Wind generator stability enhancement by using an adaptive artificial neural network –controlled superconducting magnetic energy storage," *In the Proc. Of IEEE International Conference on Electrical Machines and Systems, (ICEMS)*, Sapporo, Japan, October 2012.
[15] S.M. Muyeen, Hany M. Hasanien, and Ahmed Al-Durra, "Transient stability enhancement of wind farms connected to a multi-machine power system by using an adaptive ANN-controlled SMES," *Energy Conversion and Management*, vol. 78, no. 2, pp. 412-420, Feb. 2014.
[16] Hany M. Hasanien, and S. M. Muyeen, "Design optimization of controller parameters used in variable speed wind energy conversion system by genetic algorithms", *IEEE Transactions on Sustainable Energy*, vol. 3, no. 2, pp. 200-208, April 2012.
[17] Hany M. Hasanien, and S. M. Muyeen, "A Taguchi approach for optimum design of proportional-integral controllers in cascaded control scheme", *IEEE Transactions on Power Systems*, vol. 28, no. 2, pp. 1636–1644, May 2013.
[18] Hany M. Hasanien, "Design optimization of PID controller in automatic voltage regulator system using Taguchi combined genetic algorithm method", *IEEE Systems Journal*, vol. 7, no. 4, pp. 825-831, December 2013.
[19] Hany M. Hasanien, "Shuffled frog leaping algorithm-based static synchronous compensator for transient stability improvement of a grid-connected wind farm", *IET Renewable Power Generation*, vol. 8, no. 6, pp. 722-730, August 2014.
[20] D. J. Trudnowski, A. Gentile, J. M. Khan, and E. M. Petritz, "Fixed-speed wind generator and wind-park modeling for transient stability studies," *IEEE Transactions on Power Systems*, vol. 19, no. 4, pp. 1911–1917, 2004.
[21] S. Heier, "Grid integration of wind energy conversion system," Chicester, U.K., John Wiley & Sons Ltd., 1998.
[22] S.M. Muyeen, Hany M. Hasanien, and J. Tamura, "Reduction of frequency fluctuation for wind farm connected power systems by an adaptive artificial neural network controlled energy capacitor system", *IET Renewable Power Generation*, vol. 6, no. 4, pp. 226-235, July 2012.
[23] S. Ravichandran, K. Devi, and S. G. Bharathidasan, "Coordinated controller design of grid-connected variable-speed wind energy conversion system with model-based predictive control using response surface methodology", *Electric Power Components and Systems*, vol. 42, no. 11, pp. 1107-1120, August 2014.
[24] S. G. Varzaneh, H. Rastegar, and G. B. Gharehpetian, "A new three-mode maximum power point tracking algorithm for doubly fed induction generator based wind energy conversion system", *Electric Power Components and Systems*, vol. 42, no. 1, pp. 45-59, January 2014.
[25] P. M. Anderson and A. Bose, "Stability simulation of wind turbine systems," *IEEE Transactions on Power Apparatus and Systems*, vol. PAS-102, no.12, pp.3791-3795, December 1983.
[26] Hany M. Hasanien, Ahmed S. Abd-Rabou, and Sohier. M. Sakr, "Design optimization of transverse flux linear motor for weight reduction and performance improvement using response surface methodology and genetic algorithms," *IEEE Transactions on Energy Conversion*, vol. 25, no. 3, pp. 598-605, September 2010.

[27] PSCAD/EMTDC Manual, Manitoba HVDC Research Center, 1994.
[28] J. Kennedy and R. Eberhart, "Particle swarm optimization," *in Proc. IEEE International Conference of Neural Networks (ICNN)*, vol. 4, pp. 1942-1948, Nov. 1995.
[29] Na He, Dianguo Xu, and Lina Huang, "The application of particle swarm optimization to passive and hybrid active power filter design," *IEEE Transactions on Industrial Electronics*, vol. 56, no. 8, pp. 2841-2851, August 2009.
[30] Chien-Hung Liu and Yuan-Yih Hsu, "Design of a self-tuning PI controller for a STATCOM using particle swarm optimization," *IEEE Transactions on Industrial Electronics*, vol. 57, no. 2, pp. 702-715, Feb. 2010.
[31] T. O. Ting, M. V. C. Rao and C. K. Loo, "A Novel approach for unit commitment problem via an effective hybrid Particle swarm optimization," *IEEE Transactions on Power Systems*, vol. 21, no. 1, pp. 411-418, Feb. 2006.
[32] Hany M. Hasanien, "Particle swarm design optimization of transverse flux linear motor for weight reduction and improvement of thrust force," *IEEE Transactions on Industrial Electronics*, vol. 58, no. 9, pp. 4048-4056, September 2011.
[33] M. R. AlRashidi and M. E. El-Hawary, "A Survey of particle swarm optimization applications in electric power systems," *IEEE Transactions on Evolutionary Computation*, vol. 13, no. 4, pp. 913-918, August 2009.
[34] Minitab, Minitab Inc. 2012, US.
[35] Release 2010 b, "MATLAB Optimization Toolbox," The Math Works press, August 2010.

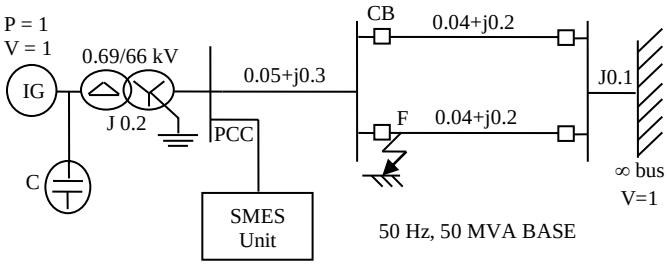

Fig. 1(a). Model system.

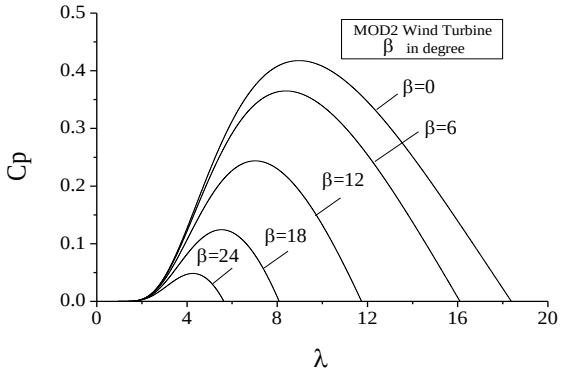

Fig. 1(b). C_P- λ characteristics for different pitch angles

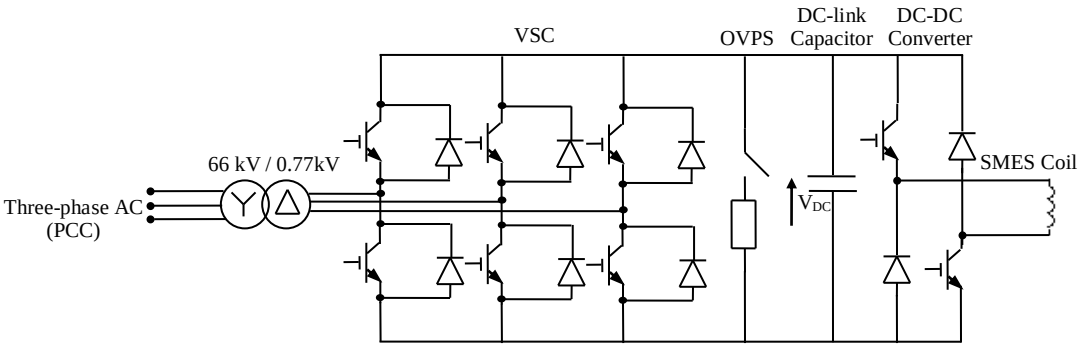

Fig. 2. SMES unit.

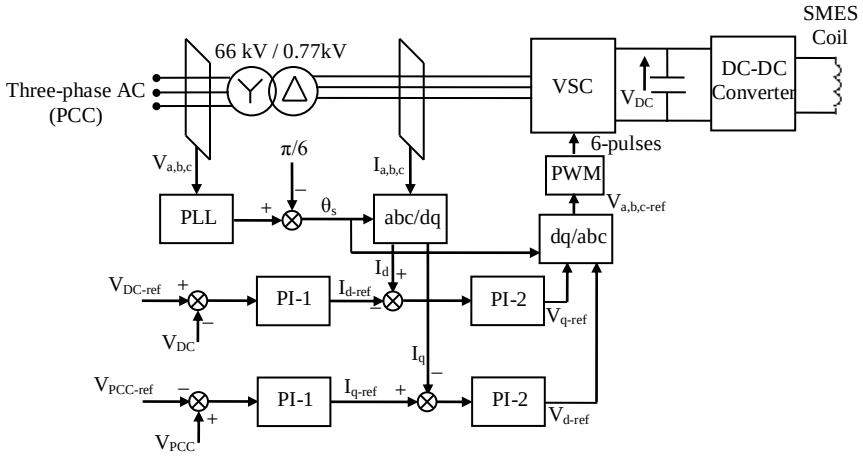

Fig. 3(a). Control block diagram of the VSC.

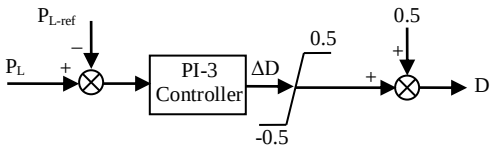

Fig. 3(b). Duty cycle control of the DC-DC converter.

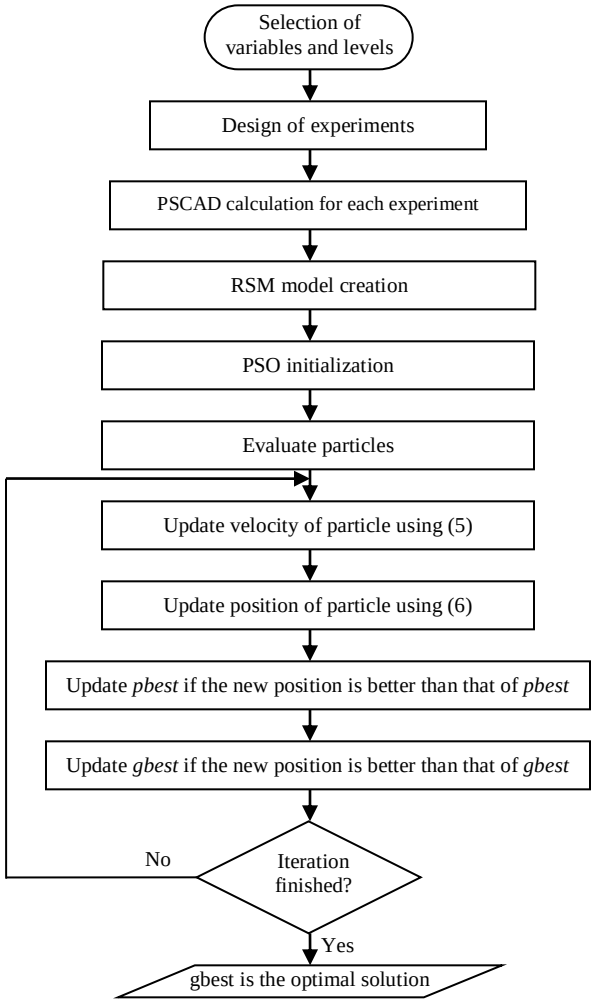

Fig. 4. Flowchart of the proposed PSO approach.

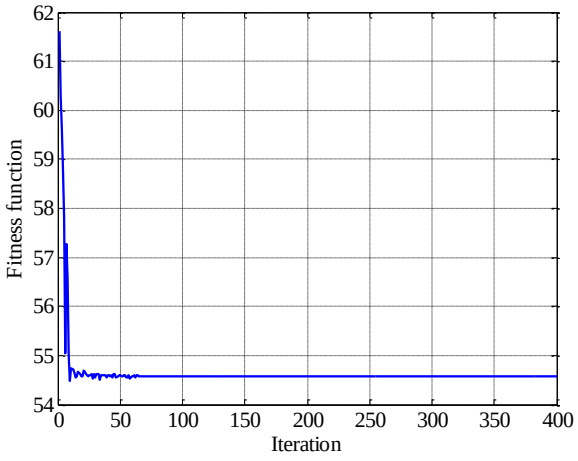

Fig. 5. Fitness function convergence using PSO.

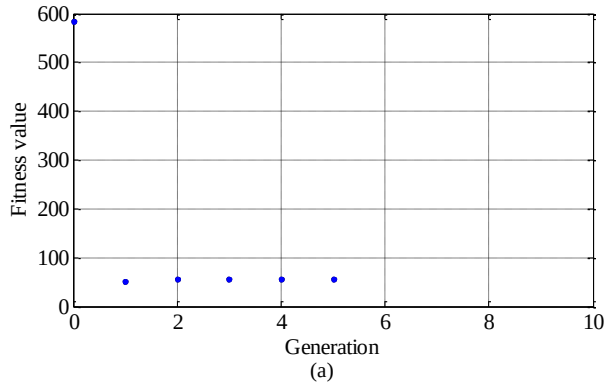

(a)

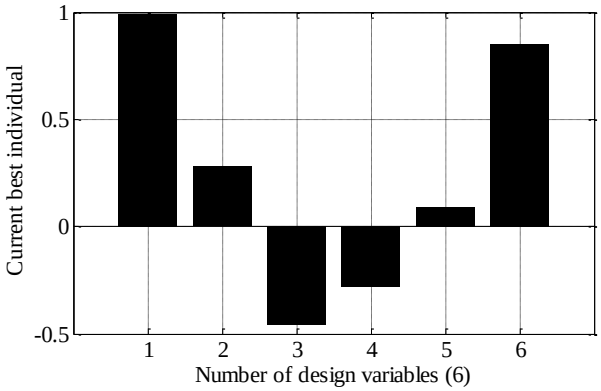

(b)

Fig. 6. (a) Fitness function convergence. (b) Current best individual.

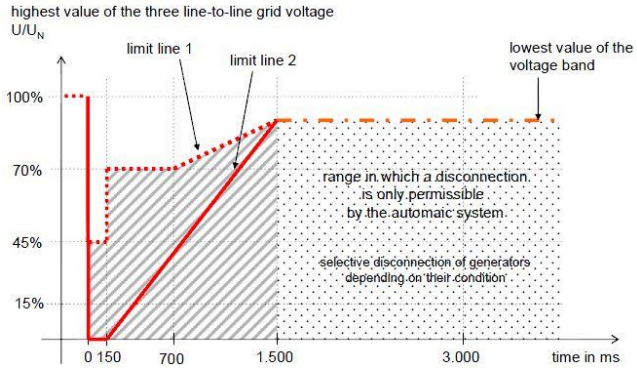

Fig. 7. LVRT standard set by E. On Netz [3].

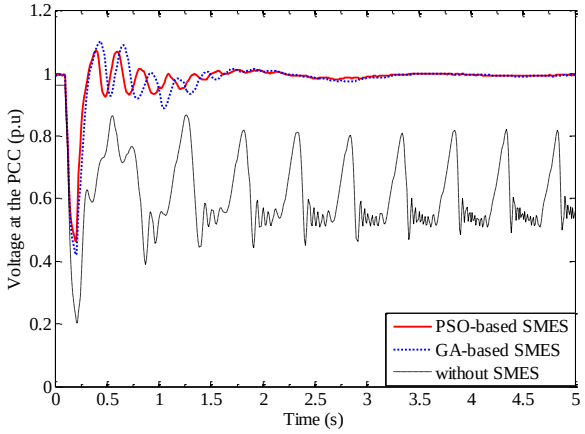
Voltage at the PCC (p.u)
Time (s)
PSO-based SMES
GA-based SMES
without SMES

(a)

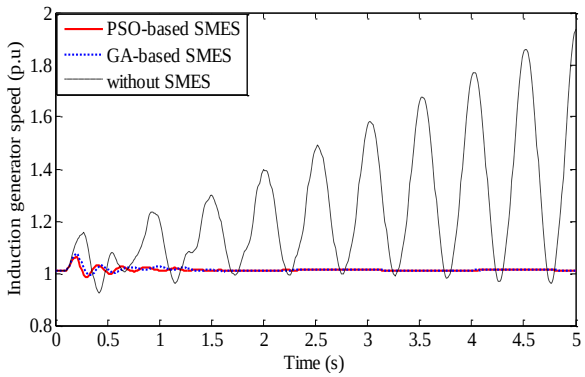
Induction generator speed (p.u)
Time (s)
PSO-based SMES
GA-based SMES
without SMES

(b)

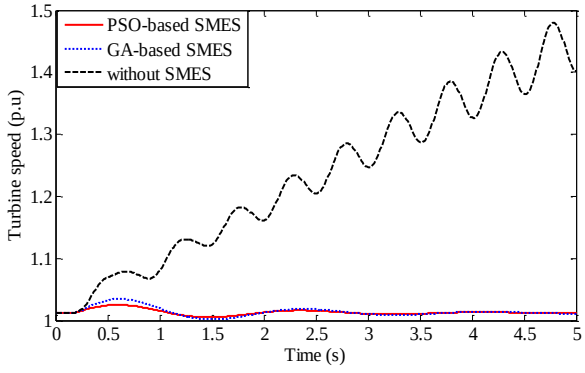
Turbine speed (p.u)
Time (s)
PSO-based SMES
GA-based SMES
without SMES

(c)

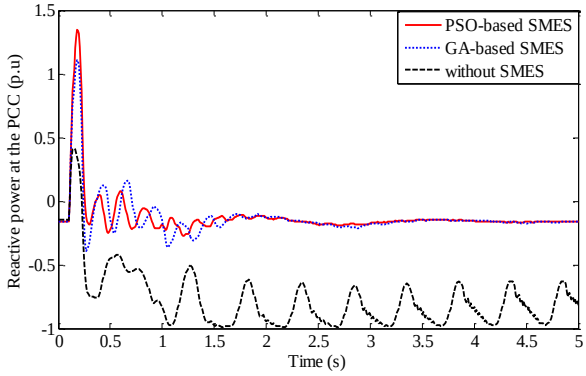
PSO-based SMES
GA-based SMES
without SMES
Reactive power at the PCC (p.u)
Time (s)

(d)

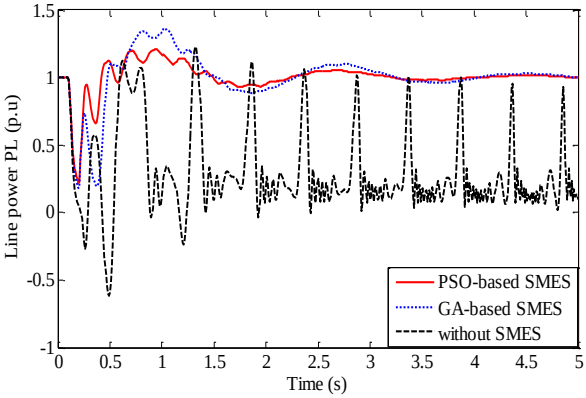
PSO-based SMES
GA-based SMES
without SMES
Line power PL (p.u)
Time (s)

(e)

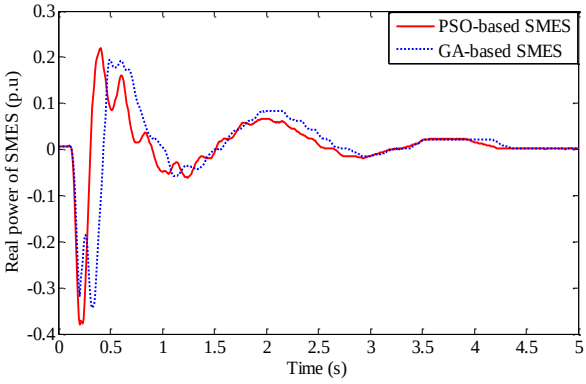
PSO-based SMES
GA-based SMES
Real power of SMES (p.u)
Time (s)

(f)

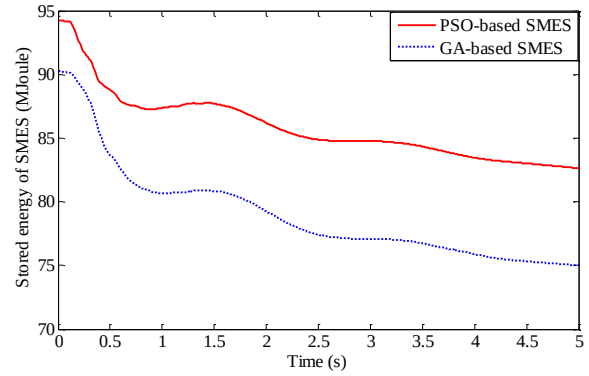

(g)

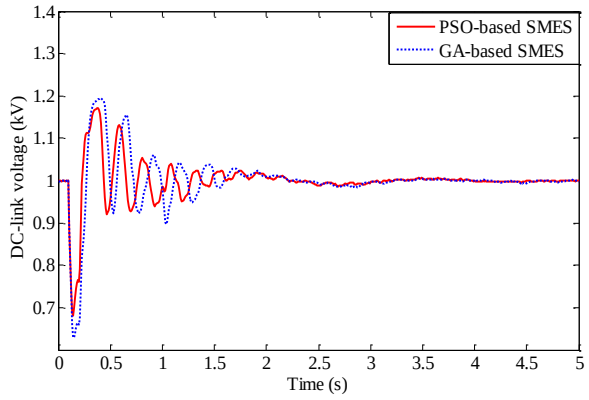

(h)

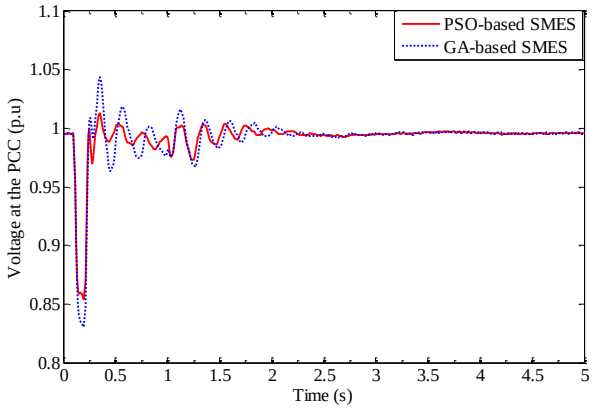

(i)

Fig. 8. Responses for 3LG fault (a) Terminal voltage at the PCC (b) Induction generator speed (c) Turbine speed (d) Reactive power at the PCC (e) Line real power at the PCC (f) Real power of SMES (g) Stored energy of SMES (h) DC-link voltage. (i) Terminal voltage at the PCC for 1LG fault.

Table I
INDUCTION GENERATOR AND TURBINE DATA

MVA	50
r_1 [pu]	0.01
x_1 [pu]	0.1
x_{mu} [pu]	3.5
r_2 [pu]	0.015
x_2 [pu]	0.12
H_g [pu]	0.3
H_{wt} [pu]	3.0
K_w [pu]	90

TABLE II
DESIGN VARIABLES AND LEVELS

Design variables Level	X_1	X_2	X_3	X_4	X_5	X_6
-1	3	0.08	1	0.001	0.1	0.002
0	4	0.1	1.5	0.002	0.6	0.251
1	5	0.12	2	0.003	1.1	0.5

TABLE III
RANGE OF DESIGN VARIABLES AND EXPERIMENT FREQUENCY

Exp. No.	X1	X2	X3	X4	X5	X6	MPUS (%)	MPOS (%)	Ts (s)	Exp. No.	X1	X2	X3	X4	X5	X6	MPUS (%)	MPOS (%)	Ts (s)
1	3	0.12	1.5	0.001	0.6	0.251	56.5	11.1	2.8	28	3	0.1	1.5	0.003	1.1	0.251	51	16	2.14
2	4	0.1	1	0.001	0.6	0.5	59	8.3	2.92	29	5	0.1	2	0.002	0.6	0.002	48	13.1	2
3	5	0.1	2	0.002	0.6	0.5	58	12	2.75	30	4	0.1	2	0.003	0.6	0.5	58	16.6	7
4	5	0.1	1.5	0.001	0.1	0.251	64	7.5	2.8	31	3	0.1	1	0.002	0.6	0.002	48	13.6	3
5	3	0.1	2	0.002	0.6	0.5	57.5	15	3.9	32	4	0.1	1	0.003	0.6	0.5	57.5	16	12
6	4	0.1	1.5	0.002	0.6	0.251	56	12.85	2.85	33	4	0.12	1.5	0.002	0.1	0.002	48	13.2	2.8
7	5	0.12	1.5	0.001	0.6	0.251	58.5	6.9	1.5	34	4	0.08	2	0.002	0.1	0.251	63	14.2	2.62
8	4	0.1	2	0.001	0.6	0.5	59	9	1.85	35	4	0.1	1.5	0.002	0.6	0.251	56	12.85	2.85
9	3	0.08	1.5	0.001	0.6	0.251	57	11.8	2.8	36	4	0.08	1.5	0.002	1.1	0.002	48	13.64	2.8
10	3	0.1	2	0.002	0.6	0.002	48	14.5	2.9	37	4	0.12	1	0.002	0.1	0.251	62.5	12.6	2.5
11	4	0.12	2	0.002	0.1	0.251	62.5	13.5	2.71	38	4	0.1	1.5	0.002	0.6	0.251	56	12.85	2.85
12	4	0.1	1.5	0.002	0.6	0.251	56	12.85	2.85	39	3	0.1	1	0.002	0.6	0.5	58	14.4	15
13	3	0.1	1.5	0.003	0.1	0.251	62	23	12	40	4	0.12	1	0.002	1.1	0.251	51	12.6	2.9
14	4	0.1	1	0.001	0.6	0.002	48	10.5	2.75	41	4	0.08	1	0.002	0.1	0.251	63	13.2	3.8
15	5	0.12	1.5	0.003	0.6	0.251	56	14.1	1.45	42	4	0.08	1.5	0.002	0.1	0.5	63	14.6	14
16	4	0.12	1.5	0.002	1.1	0.002	48	13.2	2.8	43	4	0.1	2	0.001	0.6	0.002	48.2	11.4	2
17	5	0.08	1.5	0.001	0.6	0.251	58.5	8	1.48	44	4	0.08	1.5	0.002	1.1	0.5	52.5	13.1	3
18	5	0.1	1	0.002	0.6	0.002	48	12.3	2.82	45	5	0.1	1.5	0.003	1.1	0.251	50.75	14.3	2.85
19	4	0.08	1	0.002	1.1	0.251	51	13	2.9	46	4	0.12	2	0.002	1.1	0.251	51	13.4	2.9
20	4	0.1	2	0.003	0.6	0.002	48	15.25	2.9	47	3	0.1	1.5	0.001	1.1	0.251	51.2	11.75	1.7
21	4	0.08	2	0.002	1.1	0.251	51	14	2.84	48	3	0.08	1.5	0.003	0.6	0.251	56	17.8	15
22	4	0.12	1.5	0.002	1.1	0.5	52	12.5	2.98	49	4	0.1	1.5	0.002	0.6	0.251	56	12.85	2.85
23	4	0.1	1	0.003	0.6	0.002	48	14.5	2.95	50	5	0.1	1.5	0.001	1.1	0.251	52.6	8.3	1.65
24	4	0.1	1.5	0.002	0.6	0.251	56	12.85	2.85	51	5	0.1	1	0.002	0.6	0.5	58	10.9	2.05
25	5	0.1	1.5	0.003	0.1	0.251	62.5	15.5	12	52	4	0.12	1.5	0.002	1.1	0.5	52	12.5	3
26	4	0.08	1.5	0.002	0.1	0.002	48	13.6	2.8	53	5	0.08	1.5	0.003	0.6	0.251	56	14.7	1.78
27	3	0.12	1.5	0.003	0.6	0.251	56	17	12	54	3	0.1	1.5	0.001	0.1	0.251	63	11.5	1.55

TABLE IV
PSO CHARACTERISTICS

PSO Parameters	
Number of particles	50
Initial velocity of the agent	0.0
Inertia weight	1
Acceleration constants	2
No. of iterations	400

TABLE V
OPTIMAL LEVEL AND SIZE OF DESIGN VARIABLES

Design variables Level	X_1	X_2	X_3	X_4	X_5	X_6
Optimum level (PSO)	1	0	-0.3	-1	0.99	0.55
Optimum size (PSO)	5	0.1	1.35	0.001	1.1	0.37
Optimum level (GA)	0.99	0.283	-0.458	-0.276	0.09	0.85
Optimum size (GA)	4.99	0.105	1.27	0.002	0.64	0.463

TABLE VI
GA CHARACTERISTICS

GA Parameters	
Population type	Double vector
Population size	50
Fitness scaling function	Rank
Selection function	Uniform
Crossover fraction	0.8
Crossover function	Scattered
Migration fraction	0.2
Migration interval	20